Vortices in the classical two-dimensional anisotropic Heisenberg model

M. E. Gouvêa,* G. M. Wysin,† and A. R. Bishop
Los Alamos National Laboratory, Los Alamos, New Mexico 87545

F. G. Mertens
Physics Institute, University of Bayreuth, D-8580 Bayreuth, Federal Republic of Germany
(Received 5 December 1988)

The structure and dynamics of vortex spin configurations are considered for a two-dimensional classical Heisenberg model with easy-plane anisotropy. Using both approximate analytic methods based on a continuum description and direct numerical simulations on a discrete lattice, two types of static vortices (planar and out-of-plane) are identified. Planar (out-of-plane) vortices are stable below (above) a critical anisotropy. The structure of moving vortices is calculated approximately in a continuum limit. Vortex-vortex interactions are investigated numerically. A phenomenology for dynamic structure factors is developed based on a dilute gas of mobile vortices above the Kosterlitz-Thouless transition. This yields a central peak scattering whose form is compared with the results of a large-scale Monte Carlo–molecular-dynamics simulation.

I. INTRODUCTION

Two-dimensional magnetism has attracted heightened interest in the past few years because of (i) the availability of much improved quasi-two-dimensional ferromagnetic and antiferromagnetic materials, including layered structures, magnetically intercalated graphite, and, most recently, Cu-based high-temperature superconductors; (ii) rapidly increasing information on spin dynamics from inelastic neutron scattering, particularly at low frequencies and long wavelength; and (iii) advances in numerical simulation capability on large lattices which can guide and test modeling of nonlinear structures and their dynamics.

Classical, anisotropic Heisenberg models are important for a large class of magnetic systems. Easy-plane (XY) symmetry is especially interesting because it admits vortexlike spin configurations and the possibility of a topological vortex-antivortex unbinding transition, as proposed by Kosterlitz and Thouless. The advances outlined above now allow us to seriously probe the dynamics associated with such a transition in real magnetic materials.

In this paper we consider the classical Heisenberg ferromagnet in two spatial dimensions and with easy-plane exchange anisotropy,

$$H=-J\sum_{(m,n)}(S_m^xS_n^x+S_m^yS_n^y+\lambda S_m^zS_n^z)\ , \tag{1.1}$$

where J is a coupling constant and the summation is taken over the nearest-neighbor square-lattice sites. Our principal concern is to understand in detail the structure and dynamics of vortex spin configurations and their signatures in dynamic structure factors, $S(\mathbf{q},\omega)$, as measured by inelastic neutron scattering.

In Sec. II we review existing literature and show that continuum theory yields two types of static vortices, viz. *"planar"* (in which spin components are confined to the XY plane) and *"out of plane"* (in which there is a pulse-shaped S_z distribution accompanying the vortex shape in S_x and S_y). In Sec. III we study these vortices via a direct numerical simulation of the discrete system (1.1), using Landau dynamics and Landau-Gilbert damping. We find a critical λ (λ_c): for $\lambda>\lambda_c$ ($<\lambda_c$) the out-of-plane (planar) vortex is stable. By studying square, triangular, and hexagonal lattices, we conjecture that λ_c increases with lattice coordination number. The exact numerical studies also support the qualitative vortex energy dependence on λ obtained in a perturbative continuum calculation.

Turning to vortex *dynamics*, an approximate analytic calculation in the continuum limit (Sec. IV) suggests that asymmetric out-of-plane spin components develop for both vortex types, with the asymmetry occurring about the direction of vortex motion. This is confirmed by numerical studies on the lattice. Preliminary numerical studies of vortex-vortex interactions (Sec. V) reveal that the anisotropy parameter λ is also important for the competition between the attractive and/or repulsive force existing between a vortex-(anti)vortex pair and the pinning forces due to the discreteness of the lattice. For $\lambda>\lambda_c$, the forces between the pair easily dominate the pinning forces of the lattice but, for $\lambda<\lambda_c$, unless the pair separation is rather small, or λ is very near λ_c, the pinning forces of the lattice are predominant.

Finally, in Sec. VI we consider a phenomenology based on a dilute gas of mobile vortices to calculate $S(\mathbf{q},\omega)$ above the Kosterlitz-Thouless transition temperature. This suggests an intrinsic *"central peak"* component (i.e., spectral weight at $\omega\sim 0$). In particular, we note that the correlation of S_z spin components $[S_{zz}(\mathbf{q},\omega)]$ is very sensitive to the vortex shape. Thus the velocity dependence of the shape noted above has a direct influence. We compare our predictions with numerical simulations on a 100×100 square lattice using a combined Monte Carlo–molecular-dynamics technique, and discuss the relevance of dynamic vortices to the observed central

peak structure. Section VII contains a summary and concluding remarks.

II. EQUATIONS OF MOTION AND STATIC SOLUTIONS

The Hamiltonian given by (1.1) reduces to the well-known isotropic Heisenberg and XY models for $\lambda=1$ and 0, respectively. The classical spin vector, $S_n=\{S_n^x,S_n^y,S_n^z\}$, can be specified by two angles of rotation θ_n and Φ_n,

$$S_n=S(\cos\theta_n\cos\Phi_n,\cos\theta_n\sin\Phi_n,\sin\theta_n)\ . \tag{2.1}$$

In a continuum approximation, Hamiltonian (1.1) can be written as

$$H=\frac{JS^2}{2}\int d^2r\left[[1-\delta(1-m^2)]\frac{(\nabla m)^2}{(1-m^2)}+(1-m^2)(\nabla\Phi)^2+4\delta m^2\right], \tag{2.2}$$

where

$$\delta=1-\lambda \tag{2.3}$$

and $m=\sin\theta$. The variables m and Φ constitute a pair of canonically conjugate variables, which means that

$$\dot{\Phi}=\frac{\partial\mathcal{H}}{\partial m},\quad \dot{m}=-\frac{\partial\mathcal{H}}{\partial\Phi}\ , \tag{2.4}$$

where $\mathcal{H}$ is the Hamiltonian density in (2.2).

The equations of motion obeyed by m and Φ can be obtained by using (2.4)

$$\frac{1}{JS}\frac{\partial m}{\partial t}=(1-m^2)\Delta\Phi-2m\nabla m\cdot\nabla\Phi\ , \tag{2.5a}$$

$$\frac{1}{JS}\frac{\partial\Phi}{\partial t}=-\frac{\Delta m}{(1-m^2)}+\delta\Delta m+m[4\delta-(\nabla\Phi)^2]-\frac{m}{(1-m^2)^2}(\nabla m)^2\ . \tag{2.5b}$$

These equations agree with the ones obtained by Takeno and Homma[1] after an appropriate change of variables is performed. Those authors presented a general theory to derive a classical spin system from the original quantum Hamiltonian for generalized Heisenberg models. However, only the one-dimensional case was studied in detail.

We are mainly interested in studying nonlinear excitations in this two-dimensional system and we will start our discussion by considering static solutions to Eqs. (2.5). Later in this paper, we will study the small distortions suffered by these objects due to their motion.

It can readily be seen that the set of expressions

$$m_p=0\ , \tag{2.6a}$$

$$\Phi_p=q\tan^{-1}(y/x),\quad q=\pm1,\pm2,\ldots \tag{2.6b}$$

corresponds to a particular solution to Eqs. (2.5). The condition expressed by (2.6a) requires $S_n^z=0$, in which case Hamiltonian (1.1) reduces to the planar model and (2.6b) describes the usual vortex of the Kosterlitz-Thouless theory. Hereafter, we will refer to this solution as a planar vortex. The energy of a single planar vortex

$$E_p=\pi JS^2\ln(R_s/r_a)\ , \tag{2.7}$$

has the well-known logarithmic dependence on R_s, the size of the system. r_a is a constant of the order of a lattice spacing and corresponds to a cutoff for the radial integration.

Another particular static solution of Eqs. (2.5) (for the two-dimensional case) has been obtained by other authors[2,3] by noticing that taking (2.6b) for Φ one can obtain a static solution of (2.5a) by requiring m to be a function of the radial polar coordinate, i.e., $m=m(r)$. The explicit expression for $m(r)$ should be obtained from the remaining equation (2.5b). Analytical (instantons) solutions for the isotropic Heisenberg model ($\lambda=1$) have been obtained by Belavin and Polyakov[4] and also by Trimper.[5] Unfortunately, Eq. (2.5b) cannot be solved analytically for general λ. However, for the conditions

$$m(r)=\begin{cases}\pm S & \text{for } r=0,\\ 0 & \text{for } r=\infty,\end{cases} \tag{2.8}$$

asymptotic solutions can be given as

$$m_{\text{out}}=\begin{cases}pS\left[1-\dfrac{a^2r^2}{2r_v^2}\right] & \text{for } r\to0, \qquad (2.9a)\\ cS\left[\dfrac{r_v}{r}\right]^{1/2}\exp(r/r_v) & \text{for } r\to\infty, \qquad (2.9b)\end{cases}$$

where $p=\pm1$ depending on the sign of m_{out} at the origin, and r_v is defined by

$$r_v=\frac{1}{2}\left[\frac{\lambda}{1-\lambda}\right]^{1/2} \tag{2.10}$$

and is interpreted as being the "radius" of the vortex core. a and c are constants that can be fitted by matching the asymptotic solutions (2.9). (If we match at $r=r_v$, we obtain $a=\pi e/5$ and $c=3\pi/10$.) Equations (2.9) were obtained for $q=\pm1$ since this is the case of main interest. We will refer to this solution as the out-of-plane vortex.

The asymptotic solutions obtained by Takeno and Homma[3] are of similar form although there are some differences between their expressions and ours, partially because they included an external field applied along the z axis. Hikami and Tsuneto[2] arrived at slightly different vortexlike solutions because they neglected the contribution of a term $\delta\sin\theta\cos\theta\nabla\theta$ in their continuum Hamiltonian. Expressions identical to those in Eqs. (2.9) were obtained by Nikiforov and Sonin[6] for the Hamiltonian

$$H=-\tilde{J}\sum_{m,n}(S_m^xS_n^x+S_m^yS_n^y+S_m^zS_n^z)-\tilde{\delta}\tilde{J}\sum_m(S_m^z)^2\ , \tag{2.11}$$

i.e., with local instead of exchange anisotropy. For this model, the vortex radius is $\tilde{r}_v=1/(2\tilde{\delta})^{1/2}$. Hamiltonians (1.1) and (2.11) become equivalent for $\lambda\to1$, $\tilde{\delta}\to0$, and, in this limit, r_v and $\tilde{r}_v$ diverge. The difference between these two models becomes greater in the opposite limit, $\lambda\to0$ and $\tilde{\delta}\to1$. In particular, we have $r_v=0$ and

$\tilde{r}_v = 1/\sqrt{2}$ for $\lambda = 0$ and $\delta = 1$, respectively.

If we insert $\lambda = 0$ into (2.5), we do not obtain a decaying solution as in Eq. (2.9b). Thus the only meaningful static vortex solution is the planar one—which is in agreement with our vortex radius definition [$r_v(\lambda = 0) = 0$]. It should be stressed that r_v is less than one lattice spacing for an appreciable range of λ ($r_v < 1$ for $\lambda \leq 0.8$). This leads us to consider whether the discrete nature of the lattice introduces effects that invalidate a continuum approach. Numerical simulation studies on a discrete lattice have been performed (Sec. III) in order to obtain information about the behavior of vortex solutions as functions of λ. In particular, we have determined the ranges of λ for which the static planar and out-of-plane vortex solutions are stable.

The energy of a single out-of-plane vortex E_{out} is calculated in the Appendix. We find that, for $\lambda \ll 0.8$, E_{out} is higher than E_p and increases with λ. This λ dependence of E_{out} is in agreement with our simulation results, presented in Sec. III.

III. SINGLE-VORTEX SIMULATIONS

In order to clarify the behavior of the two static vortex solutions identified in Sec. II as functions of the anisotropy λ and the location of the vortex center on the lattice, simulation studies were performed on a 40×40 square lattice. The discrete equations of motion used in the numerical simulations are

$$\mathbf{S}_i = \mathbf{S}_i \times \mathbf{F}_i - \epsilon \mathbf{S}_i \times (\mathbf{S}_i \times \mathbf{F}_i) , \tag{3.1}$$

$$\mathbf{F}_i = J \sum_{ij} (S_j^x \hat{\mathbf{x}} + S_j^y \hat{\mathbf{y}} + \lambda S_j^z \hat{\mathbf{z}}) . \tag{3.2}$$

The sum on j only runs over the nearest neighbors of i. The parameter ϵ is the strength of a Landau-Gilbert damping, which was included for testing vortex stability and for damping out spin waves generated from nonideal initial conditions. Neumann or free boundary conditions were used for simulating single vortices. The equations for the xyz spin components were integrated using a fourth-order Runge-Kutta scheme with a time step of 0.04 (in time unit $\hbar/JS$). Conservation of energy and spin length (to about 1 part in 10^5) served as checks of numerical accuracy.

The first set of simulations used a single planar vortex in a unit cell of the lattice as the initial condition. The equations of motion were integrated for several hundred time units, using a damping strength $\epsilon = 0.1$ for $0 \leq \lambda \leq 1$. We observe that for all $\lambda < (0.72 \pm 0.01)$, the planar vortex remains as the stable configuration; a bell-shaped out-of-plane spin component centered at the vortex center is seen to develop only for $\lambda > 0.72$. Figures 1(a), and 1(b) show the stationary long-time configuration obtained for $\lambda = 0.80$ and 0.90. They agree rather well with the asymptotic expressions given by (2.9). The radius of the area where m differs appreciably from zero—~ 3 lattice sites for $\lambda = 0.80$ [$r_v(\lambda = 0.80) = 1$] and ~ 4.5 for 0.90 [$r_v(\lambda = 0.90) = 1.5$]—increases with λ in the same way that r_v does. Fitting Eqs. (2.9) to the resulting out-of-plane structure, we obtain $a = 0.39\pi$ and $c = 0.65\pi$ which are close to the values we find when matching the asymptotic solutions at $r = r_v$ (Sec. II).

The stability of the planar vortex for small λ ($\lambda \ll 0.80$) can be established analytically by considering small perturbations, (Φ_1, m_1), to the static vortex (Φ_p, m_p). We use the ansatz

$$\Phi = \Phi_p + \Phi_1; \quad m = m_p + m_1 \tag{3.3}$$

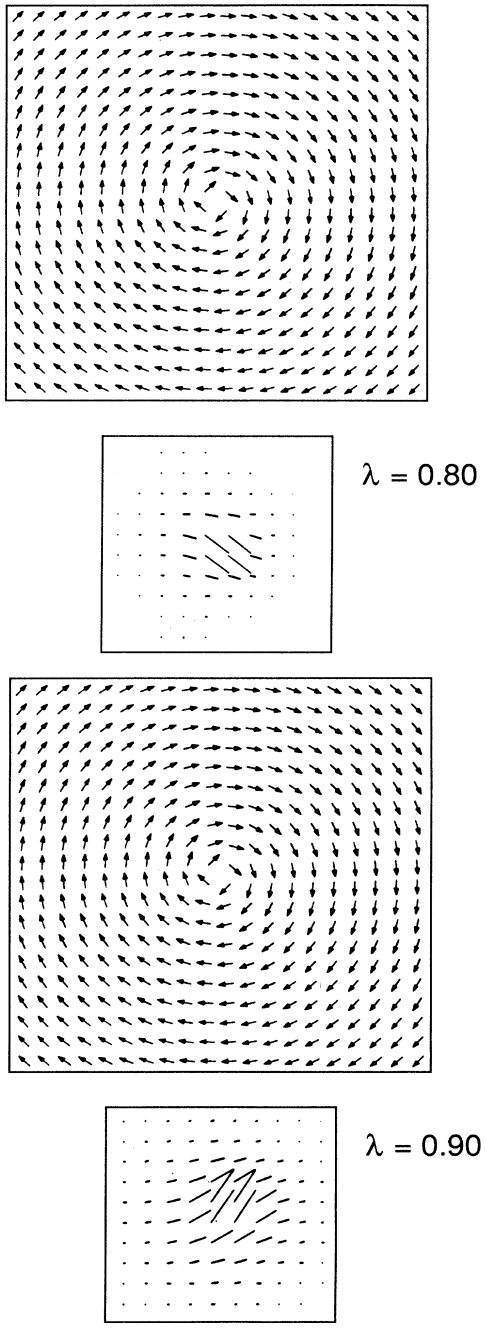

FIG. 1. Single vortex for (a) $\lambda = 0.80$ and (b) $\lambda = 0.90$ after integration time for 400 time units starting from a planar vortex ($\theta = 0$). The arrows (inside the upper square) represent the spins projected on the xy plane. The out-of-plane angles θ are shown in the lower square. The lengths of the lines are proportional to θ; the angles from the horizontal axis are θ.

in the Hamiltonian (2.2) obtaining

$$\delta H = H(\Phi,m) - H(\Phi_p,m_p) = \pi J S^2 \int_{r_a}^{R_s} r\,dr \left[\lambda(\nabla m_1)^2 + m_1^2 \left[4\delta - \frac{1}{r^2} \right] + (\nabla \Phi_1)^2 \right] . \tag{3.4}$$

The first and third terms in the integrand of (3.4) are always positive but the second term is positive only if $r > r_0$, where $r_0 = 1/\sqrt{2\delta}$. For $0 \le \lambda \le 3/4$, r_0 is inside the vortex core and integration from $r = r_a$ to R_s always yields $\delta H > 0$, i.e., the planar vortex is stable here.

Another set of single-vortex simulations was performed using a static out-of-plane vortex as initial condition. The initial configuration was specified by Eq. (2.6b) for Φ and Eq. (A3) for m (only the first two coefficients, α_1 and α_2, were taken). We find that the initial out-of-plane vortex relaxes to a planar one for $\lambda \le 0.72$. Again, only for $\lambda > 0.72$ does the out-of-plane vortex stay as a stable configuration.

Complementary simulations were performed using triangular and hexagonal lattices. Similar behaviors were found: viz., there is a "critical" value λ_c above which the static out-of-plane vortex solution is the stable configuration; for $\lambda < \lambda_c$, the stable configuration is the planar vortex. The static limit of the equations of motion derived for these nonsquare lattices leads to asymptotic solutions identical to the ones given by Eqs. (2.6) and (2.9)—this result could be expected since these equations are obtained in a continuum theory. Our numerical simulations give $\lambda_c \approx 0.62$ for the triangular lattice and $\lambda_c \approx 0.86$ for the hexagonal lattice. This suggests that the static planar vortex stability decreases with increasing coordination number.

A fourth set of single-vortex simulations using an out-of-plane vortex as initial condition but considering different positions of the vortex center was performed to give insight into how the energy of this vortex depends on the location of its center—relevant for vortex dynamics. Three positions in a square lattice were considered: (a) at the center of a square formed by four neighbors; (b) at the center of a line joining two nearest neighbors; and (c) at one of the lattice sites. For small λ, the total energy is different for each of the cases, being lowest for case (a) and highest for (c). As λ increases the differences between these energies decrease, and for $\lambda \approx 0.7$ all these energies are close to each other. The λ dependence of the energy can also be extracted from these simulations and agrees qualitatively with the behavior predicted by the calculations given in the Appendix.

IV. SINGLE MOVING VORTICES

Above the Kosterlitz-Thouless transition temperature the system is in a disordered phase characterized by unbound vortices interacting with each other. Equations of motion for single-moving vortices were derived by Huber[7] and Nikiforov and Sonin.[6] In this section we will study the distortion suffered by the static vortex solutions given in Sec. III due to their motion. The procedure chosen is the one adopted in Ref. 6 for Hamiltonian (2.11). We will also be interested in obtaining the energy of these moving vortices as a function of their velocity v.

We use an ansatz similar to the one given by Eqs. (2.2) writing

$$\Phi = \Phi_0 + \Phi_1, \quad m = m_0 + m_1 , \tag{4.1}$$

where (Φ_0, m_0) denote the static solutions given by Eqs. (2.6) and (2.9) and (Φ_1, m_1) are the distortions (assumed small) due to the vortex motion. Inserting (4.1) into (2.5), we obtain

$$-\frac{\mathbf{v}\cdot\nabla\Phi_0}{JS} = \frac{\Delta m_1}{(1-m_0^2)} - \delta \Delta m_1 + \left[\frac{2m_0 \Delta m_0}{(1-m_0^2)^2} - [4\delta - (\nabla\Phi_0)^2] + \frac{4m_0^2(\nabla m_0)^2}{(1-m_0^2)^3} + \frac{(\nabla m_0)^2}{(1-m_0^2)^2} \right] m_1 + 2m_0 \nabla\Phi_0 \cdot \nabla\Phi_1 + \frac{2m_0}{(1-m_0^2)^2} \nabla m_0 \cdot \nabla m_1 , \tag{4.2a}$$

$$-\frac{\mathbf{v}\cdot\nabla m_0}{JS} = (1-m_0^2)\Delta\Phi_1 - 2m_0 \nabla m_0 \cdot \nabla m_1 - 2m_0 \nabla m_1 \cdot \nabla \Phi_0 , \tag{4.2b}$$

after linearizing in m_1, Φ_1 and also in $\mathbf{v}$. In Eqs. (4.2) we have used

$$\frac{\partial \Phi}{\partial t} = -\mathbf{v}\cdot\nabla\Phi, \quad \frac{\partial m}{\partial t} = -\mathbf{v}\cdot\nabla m \tag{4.3}$$

for a steady-state vortex motion with velocity $\mathbf{v}$.

It is clear from Eqs. (2.5) that a moving vortex cannot be confined to the XY plane. The moving structure must develop some out-of-plane spin component. Using Eqs. (2.6) into (4.2) we have

$$-\frac{\mathbf{v}\cdot\hat{\mathbf{e}}_\phi}{JSr} = -\lambda \Delta m_{1P} + m_{1P} \left[4\delta - \frac{1}{r^2} \right] , \tag{4.4a}$$

$$0 = \Delta \Phi_{1P} , \tag{4.4b}$$

where $\hat{\mathbf{e}}_\phi$ is the unit vector for the ϕ coordinate. A particular solution of Eq. (4.4b) is given by $\Phi_{1P} = 0$ and the asymptotic behavior of m_{1P} can be obtained from Eq. (4.4a),

$$m_{1P}=\begin{cases}\dfrac{\mathbf{v}\cdot\hat{\mathbf{e}}_\phi}{JS}r=-\dfrac{v}{JS}r\sin(\phi-\alpha), & r\to 0 \quad (4.5a)\\ -\dfrac{\mathbf{v}\cdot\hat{\mathbf{e}}_\phi}{4\delta JS}\dfrac{1}{r}=\dfrac{v}{4\delta JS}\dfrac{\sin(\phi-\alpha)}{r}, & r\to\infty \quad (4.5b)\end{cases}$$

where α is the angle between the direction of the velocity $\mathbf{v}$ and the x axis. We notice that the moving vortex does not possess the circular symmetry exhibited by the static vortex since it depends on the polar coordinate ϕ and is symmetric about the $\mathbf{v}$ direction. This symmetry could be expected if we want the profile to define a distinct direction for the velocity and is confirmed by our vortex-antivortex pair simulation (Sec. V). We note that Eq. (4.4a) can be solved exactly in the $\lambda=0$ limit leading to

$$m_{1P}=\frac{v}{JS}\frac{r\sin(\phi-\alpha)}{4\delta r^2-1}\ , \tag{4.6}$$

which has the asymptotic behavior predicted by Eqs. (4.5). The above equation is an exact solution to (4.4a) only for $\delta=1$ but we can expect that it is a good approximation for $\delta\approx 1$. Equation (1.6) has a singularity (and changes sign) at $r^*=(1/4\delta)^{1/2}$ which for $\delta\approx 1$ is less than a lattice constant away from the vortex center. It is reasonable to assume that keeping the neglected nonlinear terms would suppress the divergence and force m_{1P} to cross zero near r^* to justify the assumption of small spatial derivatives. The reliability of our asymptotic $r\to 0$ solution is questionable but this will not affect our calculations because this solution will be used only in a negligible regime [$0<r<r_v$ and $r_v<1$ for $\lambda<0.8$]. Also, we will be interested in correlation functions for small q only (Sec. VI) where the asymptotic $r\to\infty$ solution is sufficient. Nevertheless, this question will be properly handled using a numerical simulation (Sec. V).

Asymptotic expressions for the small corrections to the out-of-plane vortex due to its motion can be determined by substituting Eqs. (2.6b) and (2.9) into Eqs. (4.2). We obtain

$$m_{1OP}=-\frac{a^2v}{3JS}r^3\sin(\phi-\alpha)\ , \tag{4.7a}$$

$$\Phi_{1OP}=p\frac{v}{JS}r\cos(\phi-\alpha)\ , \tag{4.7b}$$

for $r\to 0$ and

$$m_{1OP}=\frac{v}{4\delta JS}\frac{\sin(\phi-\alpha)}{r}\ , \tag{4.7c}$$

$$\Phi_{1OP}=\frac{cvr_v^{3/2}}{JS}\frac{e^{-r/r_v}v\cos(\phi-\alpha)}{r^{1/2}}\ , \tag{4.7d}$$

for $r\to\infty$. As before, the out-of-plane component m is asymmetric about the direction of motion but now this asymmetry is a small correction to be added to the core shape given by Eq. (2.9a), while in the previous case, Eq. (4.5) corresponds to the predicted shape for the out-of-plane component of a vortex moving with small velocities. The motion also destroys the circular symmetry of the in-plane component. If the procedure we have adopted is a good approximation, the vortex radius will not be strongly affected by the motion.

The energy of the moving vortex given by Eqs. (4.5) can be evaluated using Hamiltonian (2.3). For small λ, we can use Eq. (4.5b) and expand the integrand in Eq. (2.3) obtaining

$$E_{MP}=E_P+\frac{\pi v^2}{8\delta J}\ln(R_s/r_a)\ , \tag{4.8}$$

which is valid only in the low-velocity regime. According to Eq. (4.8), the energy of this moving planar vortex E_{MP} increases with its velocity.

The energy of a moving out-of-plane vortex, i.e., the one specified by Eqs. (2.9), (4.1), and (4.7), is calculated by the same procedure. Keeping terms up to second order in m_{1OP} and Φ_{1OP}, we obtain from Eq. (2.3)

$$E_{MOP}=E_{out}+\frac{JS^2}{2}\int d^2r\left[\frac{(\nabla m_{1OP})^2}{(1-m_0^2)}-\delta(\nabla m_{1OP})^2+(1-m_0^2)(\nabla\Phi_{1OP})^2+\left[4\delta-\frac{1}{r^2}\right]m_{1OP}^2\right.$$
$$\left.-\frac{(\nabla m_0)^2}{(1-m_0^2)}m_{1OP}^2-4m_0\frac{\nabla m_0\cdot\nabla m_{1OP}}{(1-m_0^2)^2}m_{1OP}-4m_0m_{1OP}\nabla\Phi_0\cdot\nabla\Phi_{1OP}\right]\ , \tag{4.9}$$

where m_0 is the static out-of-plane vortex solution. The terms in first order in m_{1OP} and Φ_{1OP} are not shown in Eq. (4.9) because they give zero contribution to the energy. Here we will be interested in $\lambda>\lambda_c$. The calculation is straightforward and gives

$$E_{MOP}=E_{out}+\frac{\pi v^2}{4J}\left[\frac{1}{2\delta}\ln(R_s/r_v)+\frac{2c^2}{e^2}r_v^2+\frac{3a^2r_v^2}{2}-\frac{2a^4}{3}\left[\frac{41-39\lambda}{12}+\frac{\delta r_v^2}{a^2}\right]r_v^2\right]\ , \tag{4.10}$$

where the logarithmic term is clearly the dominant one. Thus, the energy of a moving out-of-plane vortex increases with the velocity in essentially the same way as the energy of a moving planar vortex.

V. VORTEX-ANTIVORTEX PAIR SIMULATION

In thermodynamic equilibrium a given vortex (or antivortex) will be influenced by neighboring vortices, and the idealized simulations of isolated vortices in Sec. III are oversimplified. We can make an attempt to understand vortex-vortex or vortex-antivortex interactions by simulations of isolated pairs (either vortex-antivortex or vortex-vortex). Here we report on vortex-antivortex simulations. The results of these simulations may give insight into how the interactions lead to corrections to ideal gas phenomenologies. In particular, vortex pair

simulations provide an opportunity for observing attractive forces and, additionally, forces transverse to the line connecting the centers of the pair. Such a transverse force has been suggested by Huber [Eq. (2.2) of Ref. 7]. These simulations also can indicate how the stability of a planar or out-of-plane vortex might be affected by the fields of neighboring vortices. Finally, we note that this is an attempt to generate out-of-plane vortex profiles due to the motion. These profiles can be fitted to analytic expressions for moving vortices, such as those derived in Sec. IV.

We consider simulations where the initial condition is a planar vortex-planar antivortex pair, separated by a distance r_0 between their centers

$$\phi = \tan^{-1}\left[\frac{y}{x+r_0/2}\right] - \tan^{-1}\left[\frac{y}{x-r_0/2}\right] . \quad (5.1)$$

A square lattice of side $R=100$ with periodic-boundary conditions was used. For a large initial separation, $r_0 \approx R/2$, the equations of motion with damping strength $\epsilon=0.1$, were integrated out to time $t=400$ units. (The damping produces a slowing down of the motion and leads, eventually, to annihilation of the vortex pair.) We find that the behavior of the solutions depends on whether $\lambda \geq 0.8$ or $\lambda \leq 0.7$. In either case, there is an initial relaxation of the configuration on the *boundaries* because the initial condition used involved an expression for a pair in an infinite system, which necessarily was spatially truncated to fit on a finite system. During this initial boundary adjustment period of about 10 time units, the total system energy decreases because of the damping, while the configuration reorganizes slightly to adapt itself to the finite system size. During this short-time relaxation, the pair remains planar, so that near $t=10$ we have a configuration for a planar pair confined in a finite system. The longer times of the simulation can be thought of as testing the stability of this confined planar pair.

We found that for $\lambda \leq 0.7$ the final configuration at $t=400$ units is essentially unchanged from the "initial" (planar pair in the finite system) configuration at $t=10$. The pair remains planar and neither vortex develops any velocity. The configuration was determined to be stable by the fact that the energy had become independent of time. It is probable that there is a weak long-range attractive force between vortex and antivortex (force decaying as $1/r$ for the XY model) that can be canceled out by pinning forces due to the discreteness of the lattice. We note that for much smaller initial separations, and $\lambda \approx 0.7$, it is possible for out-of-plane components and velocities to develop (see below).

On the other hand, for $\lambda \geq 0.8$, out-of-plane spin components develop, even for large initial separations, and the vortex and antivortex both develop velocity. In the time interval $10 < t < 100$ (Fig. 2), the out-of-plane spin components have an (anti)symmetry about the line connecting the vortex and antivortex; the z components for both vortex and antivortex are positive on one side of the line and negative on the other side. This sort of configuration is consistent with expectations for moving planar vortices as discussed in Sec. IV. The vortex and antivortex move toward each other, and at the same time they develop equal velocity components transverse to the line joining their centers. In terms of $\mathbf{q}_1$, a unit velocity vector with only a z component, whose direction is given by a right-hand rule, the direction of the transverse velocity unit vector $\mathbf{v}_{1t}$ can be given by

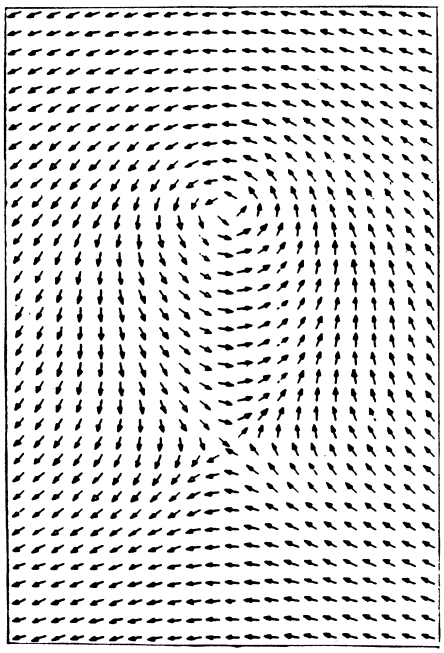

FIG. 2. Vortex-antivortex pair motion for $\lambda=0.8$ at $t=70$ starting from a planar pair [Eq. (5.1)] at $t=0$. Black and white arrows denote positive and negative out-of-plane spin component. Note the dependence of θ on the azimuthal coordinate for each vortex. Only a segment of the 100×100 lattice simulated is shown. The initial separation was 25 lattice units.

$$\mathbf{v}_{1t} = (\mathbf{r}_{12}\times\mathbf{q}_1)p_1 . \quad (5.2)$$

Subscripts 1 and 2 refer to the vortex and antivortex, respectively, and $\mathbf{r}_{12}$ is a unit vector from particle 1 to 2. p_i was defined in Eq. (2.9a). (This direction is consistent with the prediction by Huber.[7] The equation is also valid with the interchange of subscripts 1 and 2; $\mathbf{r}_{21}=-\mathbf{r}_{12}$ and $\mathbf{q}_2=-\mathbf{q}_1$, with $\mathbf{v}_{2t}=\mathbf{v}_{1t}$). For intermediate times $t>100$, the particles develop much larger out-of-plane profiles, similar to those found above in the single-vortex simulation. In this case, however, we expect that the profiles are not rotationally symmetric (Gaussian shaped), since some spatial asymmetry is necessary in order for the profile to define a specific velocity direction, as discussed in Sec. IV. A small asymmetric part exists in addition to a larger symmetric part; asymmetry is not obvious in our results, and would be difficult to measure due to large lattice discreteness effects. Estimates of the vortex radius for these moving (and interacting) vortices are comparable to those found in the single-vortex simulations. Finally, at larger times, the particles continue to move toward each other, the total energy continually decreases, and eventually, annihilation occurs.

For $\lambda=0.7$, we considered how the initial separation of

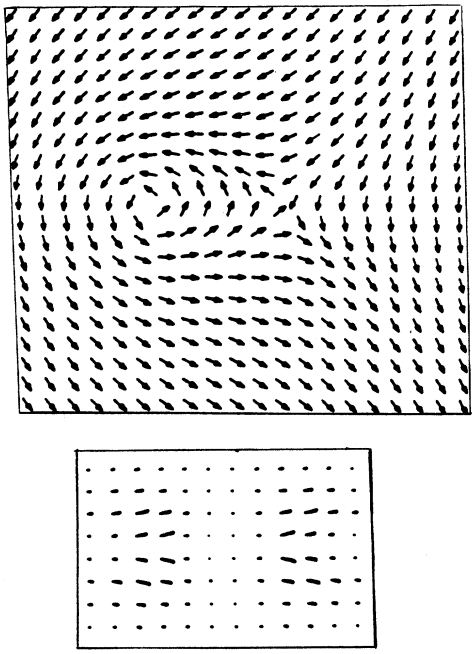

FIG. 3. Vortex-antivortex pair for $\lambda=0.7$ at $t=15$, starting from a planar pair at $t=0$ ($\theta=0$). The initial separation was 10 lattice units. Upper and lower squares as explained in Fig. 1.

the pair would influence the apparent stability of planar pair configurations seen above. We found that with initial separations $4\leq r_0\leq 10$ (Fig. 3), the pair acquired equal and opposite velocities and quickly annihilated. The out-of-plane spin components were (anti)symmetric about the line connecting the particles' centers, being positive on one side and negative on the other side (as found above for $10<t<100$ with $\lambda\geq 0.8$). The time intervals until annihilation were approximately 6, 10, 16, and 25 time units for initial separations of 4, 6, 8, and 10 lattice units, respectively. For an initial separation of 12 lattice units, the pair also acquired velocities, which became appreciable only after 200 time units, but the motion was not rectilinear. Instead, the pair acquired an orbital motion, moving through less than half a revolution in 100 time units before annihilating. Also, the out-of-plane spin components were more like those of an out-of-plane vortex as in Sec. IV. These results suggest that at small separations, the attractive forces between the pair can overcome the pinning forces due to the lattice, and there is a well-defined critical radius beyond which pinning is the dominant force.

VI. DYNAMIC FORM FACTOR FOR THE OUT-OF-PLANE CORRELATION FUNCTION

A phenomenological model has been proposed by some of us[8] to explain the dynamic properties of spin vortices in two-dimensional easy-plane ferromagnets. This phenomenology assumed an ideal, dilute gas of free vortices above the Kosterlitz-Thouless transition temperature moving in the presence of renormalized spin waves and screened by the remaining vortex-antivortex bound pairs. Using that model one can calculate the vortex contributions for the wave vector and frequency dependence of in-plane, $S_{xx}(\mathbf{q},\omega)$, and out-of-plane, $S_{zz}(\mathbf{q},\omega)$, dynamic structure functions.

The in-plane and out-of-plane correlations must be carefully distinguished:[8] the in-plane correlations are globally sensitive to the presence of vortices while the out-of-plane correlation function is sensitive to the vortex shape and size. It is clear from the previous sections that, for the XY model, the correlations of the out-of-plane spin movements must derive from moving planar vortices which have nonzero out-of-plane spin components. The previous phenomenology[8] used only the out-of-plane vortices but, as discussed earlier, out-of-plane vortices are unstable for the XY model and also for the anisotropic Heisenberg model with $\lambda\leq 0.72$. In this section, we calculate the out-of-plane correlation function, $S_{zz}(\mathbf{q},\omega)$, taking into account *moving* planar vortices. The modifications due to vortex motion affect only the vortex shape and size. The in-plane correlation function is not sensitive to these features and, for $S_{xx}(\mathbf{q},\omega)$, the results given in Ref. 8 will not be changed.

The procedure is the same as in Ref. 8. The spatial Fourier transform of the out-of-plane correlation function is given by

$$S_{zz}(\mathbf{q},t)=\frac{S^2 n_v}{(2pi)^2}\int d^2v\, P(\mathbf{v})[f(\mathbf{q},\mathbf{v})]^2 e^{-i\mathbf{q}\cdot\mathbf{v}t}\,, \tag{6.1}$$

where n_v is the density of free vortices, $P(\mathbf{v})$ is the single-vortex velocity distribution, and

$$f(\mathbf{q},\mathbf{v})=\int d^2r\, m(r) e^{-i\mathbf{q}\cdot\mathbf{r}} \tag{6.2}$$

is the velocity-dependent "vortex form factor." Any modifications concerning the vortex shape and size will directly affect this vortex form factor.

We know from previous sections that for $\lambda<\lambda_c$ the static configuration has no out-of-plane component, which gives $f(q)=0$. However, for the moving planar vortex, m is given by

$$m(r)=vg(r)\sin(\phi-\alpha)\,, \tag{6.3}$$

where $g(r)$ is some radial function whose asymptotic behavior is known (Eqs. (4.5). Inserting Eq. (6.3) into Eq. (6.2) we obtain

$$f(\mathbf{q},\mathbf{v})=i2\pi v\sin\alpha\int_0^\infty rg(r)J_1(qr)dr\,. \tag{6.4}$$

For small q, it is a good approximation to use $g(r)\sim(4\delta JSr)^{-1}$ and we obtain

$$f(\mathbf{q},\mathbf{v})=i\frac{\pi v\sin\alpha}{2\delta JS}\frac{1}{q},\quad \lambda<\lambda_c \tag{6.5}$$

and

$$S_{zz}(\mathbf{q},\omega)=\frac{n_v}{32(\delta J)^2}\frac{\bar{v}}{\pi^{1/2}q^3}e^{-[\omega^2/(\bar{v}q)^2]}\,, \tag{6.6}$$

where $\bar{v}$ is the root-mean-square velocity. $S_{zz}(\mathbf{q},\omega)$ exhibits a Gaussian central peak with width, $\Gamma_z=\bar{v}q$. The integrated intensity is

$$I_z(q)=\frac{n_v}{32\delta^2 J^2}\frac{\bar{v}^2}{q^2} . \tag{6.7}$$

The integrated intensity, as well as the form factor, diverge when $q\to 0$. This divergence occurs because we have been considering infinitely extended isolated vortices [Eq. (6.3)]. The actual radius of a vortex is limited by the presence of other vortices and therefore must be of the order of the correlation length ξ. This can be taken into account by the inclusion of a cutoff function such as $\exp[-\epsilon r/\xi]$, in the integrand of Eq. (6.4), with $\epsilon=O(1)$. Proceeding in this way we remove the $\mathbf{q}=0$ divergence, obtaining

$$\tilde{f}(\mathbf{q},\mathbf{v})=f(\mathbf{q},\mathbf{v})\chi(q) , \tag{6.8a}$$

$$\tilde{I}_z(q)=I_z(q)\chi^2(q) , \tag{6.8b}$$

where

$$\chi(q)=1-[1+(\xi q/\epsilon)^2]^{-1/2} . \tag{6.9}$$

In order to compare with the autocorrelation function of Huber[7] we integrated over $\mathbf{q}$

$$\int I_z(q)d^2q=\frac{\pi n_v \bar{v}^2}{16\delta^2 J^2}\ln(\eta\xi/a) . \tag{6.10}$$

η depends on the cutoff, e.g., $\eta=\pi/4\epsilon$ using (6.8b) for $0\le q\le \pi/a$, or $\eta=1$ if we simply restrict (6.7) to $\pi/\xi\le q\le\pi/a$.

Equation (1.12) of Huber[7] for the autocorrelation function reads in our notation

$$\langle S_n^z(t)S_n^z(0)\rangle=\frac{\pi n_v}{16\delta^2 J^2}\langle \mathbf{v}(t)\cdot\mathbf{v}(0)\rangle\ln(L/a) , \tag{6.11}$$

where a cutoff at L (size of the system) was made. Huber calculated $\langle \mathbf{v}(t)\cdot\mathbf{v}(0)\rangle$ assuming a *diffusive* rather than a ballistic motion of the vortices. Therefore the frequency dependence of the Fourier transform (footnote 28 of Ref. 7) is different from that of our central peak in (6.6). However, the integrated intensity is independent of the kind of motion and can be compared directly with our result. In fact, (6.11) for $t=0$ is identical to (6.10), apart from the logarithmic term because of the different cutoff.

For $\lambda>\lambda_c$, the main contribution to the form factor comes from the stable static out-of-plane vortex structure. The expressions for $f(q)$, $S_{zz}(q,\omega)$, and $I_z(q)$ are then those given in Ref. 8. However, the expression for the *vortex radius* must be replaced by our Eq. (2.10).

Now we compare the predictions of this theory with the results of our Monte Carlo–molecular-dynamics (MC–MD) simulations for the XY model. The simulations used a 100×100 square lattice with periodic-boundary conditions, allowing access to $q\ge 0.02(\pi/a)$. First, an MC algorithm of 10^4 steps per spin was used to produce three equilibrium configurations at a desired temperature. These were used as initial conditions for MD using fourth-order Runge-Kutta time integration with time step 0.04, sampling time $\Delta t=N_s(0.04)$, with $N_s=4$ or 8 depending on the wave vector of interest. A Gaussian window function was applied to $S(q,\omega)$ before using a fast-Fourier transform (FFT) algorithm for the Fourier transform. $S(q,\omega)$ was averaged over the three initial conditions.

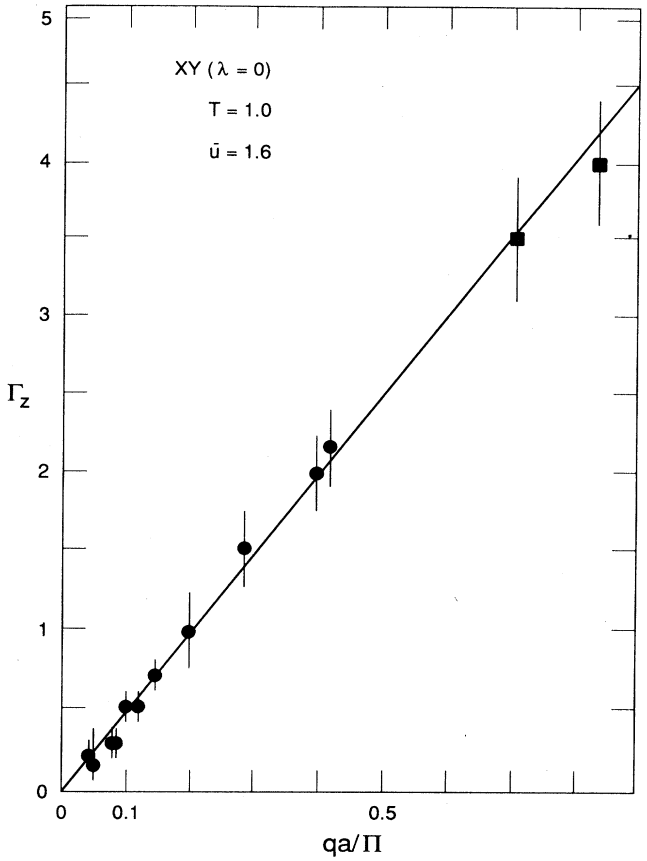

FIG. 4. Width of the central peak in $S_{zz}(\mathbf{q},\omega)$ for $T=1.0$. Data points and error bars result from estimating Γ_z from MC–MD data. The solid line represents $\Gamma_z=\bar{u}q$ (using $\bar{u}=1.6$) from the Gaussian (6.6).

The simulation data show a central peak for temperatures above $T_c\sim 0.8JS^2$. We cannot unequivocally decide whether it has a Gaussian structure but we can estimate upper bounds for its width Γ_z and intensity I_z and compare those to our predictions. The half-width q dependence, $\Gamma_z=\bar{v}q$, is very well supported by our MC–MD data (Fig. 4). Figure 5 gives the integrated intensity $I_z(q)$ as extracted from our data. The dashed line corresponds to Eq. (6.7) and the solid line to Eq. (6.8b) where we used $\epsilon=0.28$. In order to estimate the free vortex density we used[9]

$$n_v\sim(2\xi)^{-2} \tag{6.12}$$

and the values for ξ and $\bar{v}$ were taken from fittings performed in Ref. 8. We remark that the orders of magnitude for I_z agree well with our predictions for both temperatures. However, other processes can also contribute to the central peak. Likely candidates are multi-spin-wave processes and other effects due to vortex-vortex and

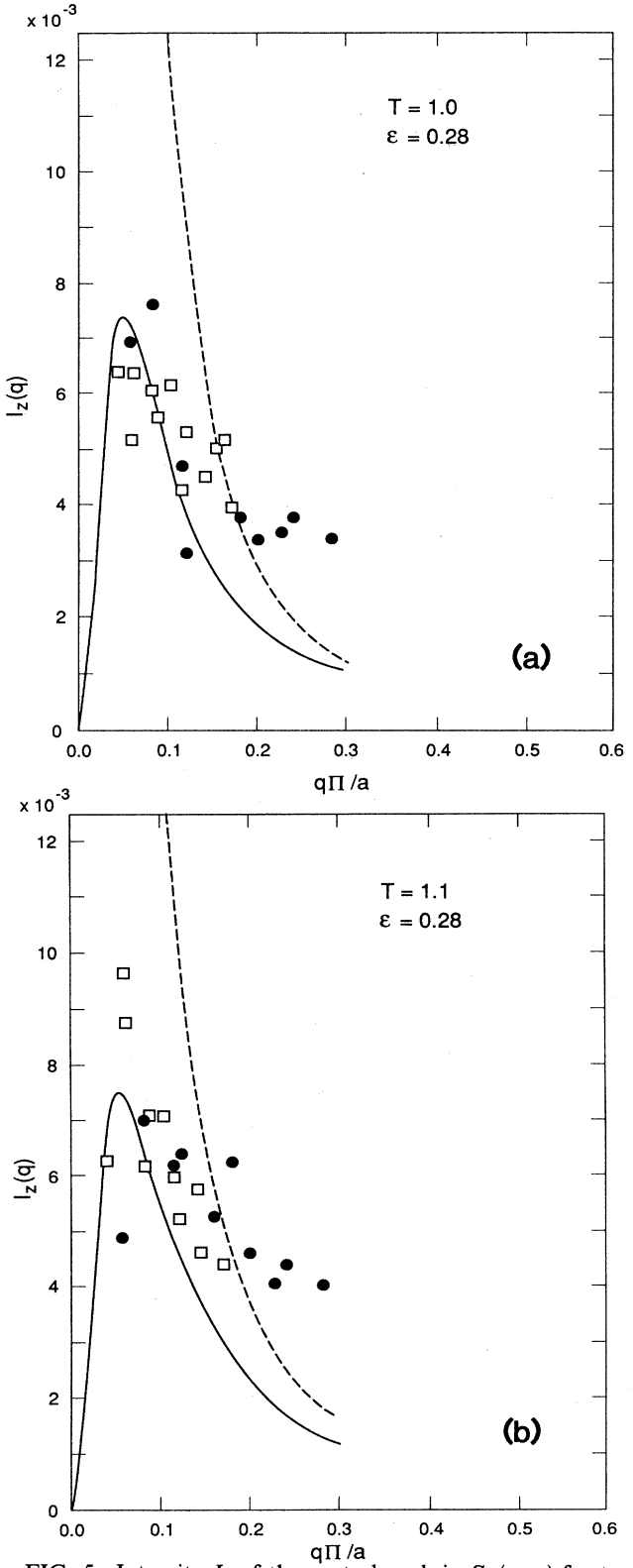

FIG. 5. Intensity I_z of the central peak in $S_{zz}(\mathbf{q},\omega)$ for two temperatures: (a) $T=1.0$ and (b) $T=1.1$. Data points result from estimating I_z from our MC–MD simulations on a 50×50 lattice (circles) and a 100×100 lattice (squares), assuming a Gaussian form of the central peak. Dashed lines represent (6.7), solid lines are fits to (6.8b) with $\epsilon=0.28$.

vortex spin-wave interactions. In particular, vortex-spin-wave interactions should become more important as the temperature increases.

VII. DISCUSSION

In this work, we study static and dynamic properties of vortices in a two-dimensional (2D) classical Heisenberg model with easy-plane anisotropy [Eq. (1.1)]. Two static vortex spin configurations, *planar* and *out of plane,* are obtained via a continuum theory. Our continuum treatment associates a parameter r_v to the out-of-plane vortex. This parameter gives an estimate of the vortex radius. However, r_v as given by Eq. (2.10), is smaller than one lattice constant for $\lambda<0.8$. Numerical simulations were performed on different discrete lattices (square, triangular, and hexagonal) and they show us that planar and out-of-plane vortices are stable configurations of the model we are considering but through distinct λ ranges; i.e., out of plane (planar) are only stable for $\lambda>\lambda_c$ ($\lambda<\lambda_c$). The critical values λ_c, obtained from our simulations, are different for each of the three lattices: $\lambda_c\approx0.62$, 0.72, and 0.86 for triangular, square, and hexagonal lattices, respectively. This λ_c behavior suggests that λ_c increases with the lattice coordination number. A continuum theory cannot explain this behavior but it is notable that the λ_c listed above are comparable to $\lambda=0.8$—the critical value we obtained from our continuum approach.

Concerning vortex dynamics, we considered how the vortex shape changes when the vortex is moving. The vortex shape is important when the correlation of S_z spin components is calculated and its modifications due to vortex movement must be taken into account. We adopted an approximate analytical treatment which assumes vortices moving at small velocities. At this time, a detailed study to determine velocities of vortices (i.e., velocity distribution functions) in models such as the one described by Eq. (1.1) has not been made and this assumption cannot be tested. However, in order to get some understanding of moving vortices, we simulated isolated vortex-antivortex pairs. These simulations qualitatively confirm our analytical results showing that an asymmetric out-of-plane structure develops. Some information concerning vortex-(anti)vortex interactions can also be extracted from these simulations. For $\lambda>\lambda_c$, effects of the out-of-plane structure on the vortex-vortex interactions can be rather strong and corrections to ideal-gas phenomenologies could be important.

For $\lambda<\lambda_c$, the effects of the out-of-plane structure are small and we assumed an ideal gas of unbound vortices with a Gaussian velocity distribution above the Kosterlitz-Thouless transition temperature to calculate out-of-plane correlations. In this λ range, the *static* vortex does not have an out-of-plane spin component and the vortex contribution to $S_{zz}(\mathbf{q},\omega)$ comes from *moving* vortices. The phenomenology predicts a Gaussian central peak for $S_{zz}(\mathbf{q},\omega)$ whose width Γ_z increases linearly with the wave-vector q. We compared our theory to MC MD simulation data obtained for the XY ($\lambda=0$) model and find good qualitative agreement. However, it is clear that

other processes must be taken into account if one wants to improve the description. Due to the *local* nature of S_{zz} correlations, we can expect that multimagnon processes and vortex-magnon interactions also give appreciable contributions to the central peak. These features have been studied by us and will be reported in future publications. On the other hand, in-plane correlations are *globally* sensitive to the presence of vortices and we believe that the main contribution is properly given (at least for $\lambda<\lambda_c$) by the phenomenological treatment of Ref. 8.

ACKNOWLEDGMENTS

One of us (M.E.G.) acknowledges CNPq (Conselho Nacional para o Desenvolvimento da Pesquisa, Brazil) for its financial support. Work at Los Alamos was performed under the auspices of the United States Department of Energy (USDOE).

APPENDIX

We will estimate the energy of a single out-of-plane vortex by using the continuum version of our Hamiltonian, Eq. (2.2). We split the integral into two contributions: one from the region inside the vortex radius, the core region, and the other from the contribution from the rest of the system,

$$H=\pi JS^2\int_0^{r_v}\mathcal{H}r\,dr+\pi JS^2\int_{r_v}^{R_s}\mathcal{H}r\,dr\ . \tag{A1}$$

Equations (2.9) correspond to only the first term of an asymptotic expansion and, in evaluating Eq. (A1), it is necessary to take into account higher-order terms so that we can find the order $(1/r^2)$ of the second term in the integrand of Eq. (2.2). One can easily verify that the expressions

$$\theta=\frac{\pi}{2}-\frac{ar}{r_v}+dr^3\cdots r\to 0\ , \tag{A2}$$

$$m=c\left[\frac{r_v}{r}\right]^{1/2}e^{-r/r_v}\left[1+\sum_{n=1}^{\infty}\alpha_n\left[\frac{r_v}{r}\right]^n\right]r\to\infty\ , \tag{A3}$$

where

$$d=\frac{\alpha\delta}{2r_v}+\frac{a^3}{12r_v^3}(1-3\delta)\ , \tag{A4}$$

$$\alpha_n=\alpha_{n-1}\frac{4+(2n-1)^2\lambda}{8\lambda n}(-1)^n\ , \tag{A5}$$

and

$$\alpha_1=\frac{4+\lambda}{8\lambda}\ , \tag{A6}$$

constitute asymptotic solutions of the equations of motion, Eqs. (2.5). The expansion (A3) does not converge, the optimal number of terms depends on r and on the λ parameter. In the denominator of each term of Eq. (A3) we have $[\lambda(1-\lambda)]^{n-2}$ and the expansion diverges in both limits, $\lambda\to 0$ and $\lambda\to 1$. (For $\lambda=0$, we have $m=0$ due to $r_v^{1/2}$ multiplying the whole expansion.) The optimal number of terms is obtained at the minimum which is approximately situated where two successive terms have the same magnitude.

For $\lambda<0.8$, we can assume that m, as well as its derivatives, are small through the whole region of integration so that the integrand in (2.3) can be expanded as

$$E_{\rm OP}=\pi JS\int_{r_a}^{R_s}r\,dr[\lambda(\nabla m)^2+4\delta m^2+(\nabla\Phi)^2(1-m^2)]\ . \tag{A7}$$

We have replaced r_v by r_a [as in (2.7)] in the lower limit of the integral. For $\lambda<0.8$, the best tractable truncation in (A3) keeps only the coefficients up to α_3. (The resulting expansion will be valid for $0.01<0.71$.) The calculation is straightforward and yields

$$E_{\rm OP}=E_P+\pi JS^2c^2r_v e^{-2r_a/r_v}\times\left[\frac{\lambda}{r_v}-\frac{4-\lambda}{4r_a}(32+322\lambda+153\lambda^2)\right] \tag{A8}$$

so that the energy $E_{\rm OP}$ increases with λ and is higher than E_P, the planar vortex energy.

For $\lambda>0.8$ the best truncation in (A3) includes only the α_1 and α_2 coefficients. Here the energy of the out-of-plane vortex is given by

$$E_{\rm OP}=E_P-\pi JS^2\left[\ln(r/r_v)+\frac{c^2}{2}(4-\lambda)-\left[2\delta+\frac{a^2}{r_v^2}\right]r_v^2+\left[2\delta+\frac{a^2}{r_v^2}+\frac{\lambda a^4}{r_v^4}\right]r_v^4\right]\ . \tag{A9}$$

$E_{\rm OP}$ is lower than E_P and decreases as λ increases.

*Permanent address: Universidade Federal de Minas Gerais, Brazil.
†Present address: Kansas State University, Manhattan, Kansas 66506.

[1]S. Takeno and S. Homma, Prog. Theor. Phys. **64**, 1193 (1980).
[2]S. Hikami and T. Tsuneto, Prog. Theor. Phys. **63**, 387 (1980).
[3]S. Takeno and S. Homma, Prog. Theor. Phys. **65**, 172 (1980).
[4]A. A. Belavin and A. M. Polyakov, Pis'ma Zh. Eksp. Teor. Fiz. **22**, 503 (1975) [JETP Lett. **22**, 245 (1975)].
[5]S. Trimper, Phys. Lett. **70A**, 114 (1979).
[6]A. V. Nikiforov and E. Sonin, Zh. Eksp. Teor. Fiz. **85**, 642 (1983) [Sov. Phys.—JETP **58**, 373 (1983)].
[7]D. L. Huber, Phys. Rev. B **26**, 3758 (1982).
[8]F. G. Mertens, A. R. Bishop, G. M. Wysin, and C. Kawabata, Phys. Rev. Lett. **59**, 117 (1987); Phys. Rev. B **39**, 591 (1989).
[9]D. G. Bishop and J. D. Reppy, Phys. Rev. Lett. **40**, 1727 (1978).